Iranica Journal of Energy & Environment

Journal Homepage: www.ijee.net

IJEE an official peer review journal of Babol Noshirvani University of Technology, ISSN:2079-2115

Near Wake Modeling of a Wind Turbine Particle Image Velocimetry Experiment

E. Mahmoodi[1]*, A. Jafari[2], A. Keyhani[2]

[1]*Department of Mechanical Engineering of Biosystems, University of Shahrood, Shahrood, Iran*
[2]*Department of Mechanical Engineering of Biosystems, University of Tehran, Alborz, Iran*

P A P E R I N F O

Paper history:
Received 17 February 2015
Accepted in revised form 1 May 2015

Keywords:
Actuator disc
Laminar Navier-Stokes
Particle image velocimetry experiment
Turbulent Navier- Stokes
Wake modeling

A B S T R A C T

In this study, different numerical models are computed and compared with particle image velocimetry (PIV) measurement for wake correlation of a 4.5 m of diameter wind turbine rotor. The collaborative European wind turbine MEXICO project is carried out in three commonly experimental defined test cases at wind speeds of 10, 15 and 24 $m.s^{-1}$. To discuss the rotor near wake, a laminar Navier-Stokes approach and a Reynolds averaged Navier-Stokes turbulent model both coupled with an actuator disc (AD) technique are computed, then compared with a direct model from the literature called TAU/DM as a full rotor technique. The actuator disc momentums are calculated using user defined functions (UDF) in FLUENT introduced as UDF/AD technique in this paper. The results are discussed in detail and compared with PIV detailed measurements.

***doi**: 10.5829/idosi.ijee.2015.06.03.07*

INTRODUCTION

Nowadays, use of renewable energy sources is highly recommended as green energy supply. Wind power is well known as environmental friendly energy source. The wind turbines are often modeled as a sink of momentum corresponding to the thrust force. The simplest models neglect terms in Navier-Stokes equations and assume the wake to be homogeneous and axisymmetric for increasing the solving speed. More wake advanced models retain all the elements of Navier-Stokes equations and model the wake and atmospheric turbulence in different ways e.g. computational fluid dynamics (CFD) with large eddy simulation (LES), Reynolds-averaged Navier-Stokes (RANS) and Reynolds-stresses model (RSM)) in a flow solver coupled with a force estimation algorithm. After computer revolution and increasing power and speed of calculations CFD is developed on 3D Navier-Stocks models [1, 2]. The rotary blade simulation based on a rotary 3D geometry meshed model in a Navier-Stokes solver (direct model: DM) suddenly made sounds in considering most of the operating conditions of the wake. A complete overview of this progression can be found in [3]. The first use of the DM technique in wind turbines is done by [4] to estimate the rotor performance of two different kinds of wind turbines. Some researchers challenge the DM technique to model the wake and flow interaction in wind farms as well as extract 3D airfoil's characteristics [5-12]. As Vermeer et al. studied on wind turbine wake aerodynamic [13], an important weakness of DM methods, despite advanced discretization techniques using high-order schemes to handle viscous and momentum fluxes, is the modeling of the wake. Some studies developed DM on MEXICO rotor experiment that exhibited interesting results on wake modeling and extraction 3D airfoil data [14, 15] and surveying the wind tunnel effects on flow circulation around the rotor [16].

A basic actuator disc is a thickless and permeable planar disc inside a streamtube. Wind speed rules as inlet on the streamtube that cause to expansion of the stream lines while cross the disc. A generalized actuator disc (AD) is a different concept of the basic one. The concept of the AD is central in the heavily used and for industrial methods is based on the blade element analysis with a multiple streamtube integral analysis. It consists in representing the rotor with an equivalent, porous surface or volume whose action on the flow is

* Corresponding author: E. Mahmoodi
E-mail: esmahmoodi@shahroodut.ac.ir

Please cite this article as: E. Mahmoodi, A. Jafari, A. Keyhani, 2015. Near Wake Modeling of a Wind Turbine Particle Image Velocimetry Experiment, Iranica Journal of Energy and Environment 6 (3): 195-206.

modeled by an associated system of forces, distributed across volumes or surfaces depending on the exact approach adopted. However, in AD-based approaches, the same limitations with respect to the wake exist since the AD technique does not model tip or root effects of the blades. As such, AD methods are more appropriate for modeling far wake effects [17]. Prandtl's tip loss correction which is a part of BEM theory [18] can be considered in the AD method as a relaxation parameter in the iterative solution process to include tip vorticity losses as finite bladed rotors [19, 20]. A wind farm is modeled by Ammara et al. [21] employing time-averaged, steady-state, incompressible Navier-Stokes equations, in which wind turbines are represented by AD approach and solved using a control-volume finite element method (CVFEM). The analysis of a two-row periodic wind farm in neutral atmospheric boundary layers using AD method demonstrated the existence of positive interference effects (Venturi effects) as well as the dominant influence of mutual interference on the performance of dense wind turbine clusters [21].

Recently, research was carried out by Rethore et al. [16, 22] that used an AD method against a DM model to study MEXICO rotor experiment and the wind tunnel effects (DNW/LLF). They used outputs of pressure sensors to feed their AD model to discuss the rotor wake. The measured pressure is integrated as momentum forces and then applied to the actuator disc nodes coupled with unsteady DES turbulence model lead to such an interesting wake simulation. Hence, wake is rising up from the measured momentums. Analytical calculation of these momentum forces via blade element analysis and airfoil formulation is considered as one of the new goals of mathematical modeling in current research.

This paper is organized in different sections. MEXICO experiment is briefly described in section 2. In section 3, a MAS technique is described; how to smooth the experimental PIV data. In section 4, the governing equations of the flow in the solution process are described. In section 5, the process of the mesh generation is cleared. In section 6, a UDF/AD technique to make a generalized actuator disc in this study is described and particular features of the rotor's blade interpolated in this study are explained. In section 7, the numerical results for both UDF/AD models are discussed in compare to MEXICO measurements. To get more assessment on the UDF/AD technique, numerical results of a direct model (full rotor) simulation from the literature [15] are included in section 7. Actually in section 8, the main conclusions of this research are presented to finalize the paper.

Mexico experiment

MEXICO wind turbine consists of a three-bladed rotor with a diameter of 4.5 m. Each blade is composed of a cylinder, the inner 4.4% of the span; a DU91-W2-250 airfoil, from 11.8 to 40% span; a RISOE-A1-21 airfoil, from 50 to 62% span and a NACA 64-418 airfoil, from 72 to 100% span, with three transitional zones between airfoils [23].

A large number of particle image velocimetry (PIV) studies were programmed to determine the flow field around the rotor, the inflow and near wake, and to track tip vortices. PIV traverse tower with two cameras, aimed at a horizontal PIV sheet (35×42 cm) in a symmetry plane of the rotor ('9 o-clocks') is illustrated in Figure. 1. Traverses used in the current study are planned in both axial and radial directions. PIV sheet is illuminated with laser flash, and two digital photographs are taken with a delay of 200 nanoseconds. Sheet is subdivided into small interrogation windows. Velocity vector is the one resulting in a maximum cross correlation between the two shots. For detail information, it is desired to address the specified literature [24].

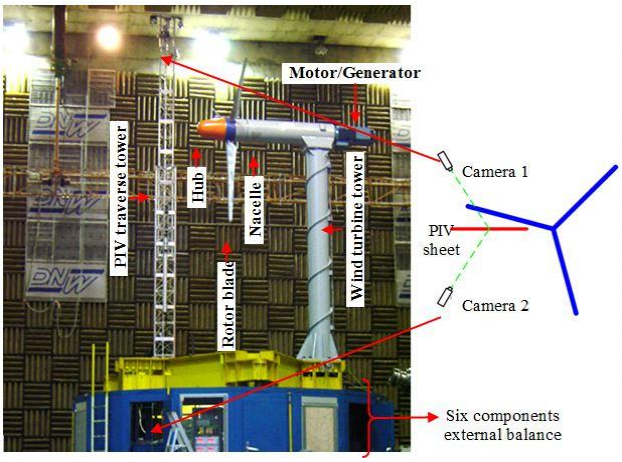

Figure 1. PIV Setup of the experiment in DNW/LLF open jet wind tunnel

The measured dataset consists of two parts. The first part is taken without the PIV measurements and is omitted in this work. Furthermore, only axisymmetric conditions are considered, i.e. conditions where the rotor is yawed have also been omitted. Three cases have been selected from a large amount (160 GB) of experimental data (run 11: point 92, point 93, point 95) [25]. The chosen measurements were performed with a wind tunnel speed of 10 (rotor turbulent state), 15 (rotor design state) and 24 $m.s^{-1}$ (rotor blade stall state), corresponding to tip speed ratios of $\lambda = 10.0$, $\lambda = 6.7$ (the design tip speed ratio) and $\lambda = 4.2$, respectively. For all measurements used in this work, the pitch angle is set at -2.3 degrees and rotor speed is set at 425.5 rpm ($\omega = 44.45$ $rad.s^{-1}$).

PIV data smoothing

The measurement data exhibit heavy transient behavior. On the other hand, mathematical models compute soft results because of time averaged depending solutions of the governing equations. Therefore, PIV data have to be smoothed for being comparable with computations. For this study, a weighted moving average smoothing (MAS) technique is used in filtering fluctuations in PIV data [26]. Equation (1) describes the MAS method in this work:

$$m_i = \frac{n_{\left(i-\frac{s-1}{2}\right)}+2n_{\left(i-\frac{s-1}{2}+1\right)}+\ldots+\left(\frac{s+1}{2}-1\right)\times n_{(i-1)}+\left(\frac{s+1}{2}\right)\times n_i+\left(\frac{s+1}{2}-1\right)\times n_{(i+1)}+\ldots+2n_{\left(i+\frac{s-1}{2}-1\right)}+n_{\left(i+\frac{s-1}{2}\right)}}{\frac{(s+1)(s+3)}{8}} \quad (1)$$

where m is the smoothed datum, n is the original datum which has to be smoothed, i is the row number and s is the span of the MAS technique. Because of the high resolution of the data, the span of MAS is set at 23 obtained from a large number of tests. This value of span describes that each n_i is smoothed via weighted 11 numbers of data before and the same after. The PIV data is smoothed twice via Equation (1) to lead to satisfactory results.

Numerical methodology

In this section, equations governing the domain solution, techniques to generate suitable meshes and methodology of the actuator disc based on UDF codes are discussed, respectively.

Flow governing equations

Conservation equations for mass and momentum have to be solved in all solutions. Equation for conservation of mass, or continuity equation, for laminar flow in an inertial (non-accelerating) reference frame, can be written as follows:

$$\frac{\partial \rho}{\partial t}+\nabla.(\rho\vec{u})=S_m \quad (2)$$

Equation (2) is the general form of the mass conservation equation and is valid for incompressible as well as compressible flows. The source S_m is the mass added to the continuous phase from the dispersed second phase. The S_m term as well as the density term ($\partial\rho/\partial t$), both are zero because of incompressible single phase flow assumption in wind energy story. Conservation of momentum in an inertial (non-accelerating) reference frame is described by following equation:

$$\frac{\partial}{\partial t}(\rho\vec{u})+\nabla.(\rho\vec{u}\vec{u})=-\nabla p+\nabla.\mu\left(\left(\nabla\vec{u}+\nabla\vec{u}^T\right)-\frac{2}{3}\nabla.\vec{u}I\right)+\vec{f} \quad (3)$$

Where p is the static pressure, $\vec{f}$ is the external body forces (e.g., that arise from interaction with the dispersed phase). The term $\mu\left(\left(\nabla\vec{u}+\nabla\vec{u}^T\right)-\frac{2}{3}\nabla.\vec{u}I\right)$ is shear stress tensor, where, μ is the molecular viscosity, I is the unit tensor, and the second term on the right hand side is the effect of volume dilation. The external body force, $\vec{f}$, contains model-dependent source terms such as porous-media or user-defined sources that are substituted by UDF source Macros in the actuator disc domain in this study. The Reynolds-averaged Navier-Stokes (RANS) equations govern the transport of the averaged flow quantities, with the whole range of the scales of turbulence being modeled. The RANS-based modeling approach therefore greatly reduces the required computational effort and resources, and is widely adopted for practical engineering applications. RANS methods aim for a statistical description of the flow that is stated as follows:

$$\frac{\partial}{\partial t}(\rho\vec{u})+\nabla.(\rho\vec{u}\vec{u})=-\nabla p+\nabla.\left(\rho(\nu+\nu_T)\left(\nabla\vec{u}+\nabla\vec{u}^T\right)\right)+\vec{f} \quad (4)$$

where ν_T is turbulent eddy viscosity. Many different turbulence models have been used by researchers to calculate eddy viscosity. The standard k-ε model is a two equation model often encountered in wind-energy wake applications [27]. Therefore a standard k-ε turbulent model is used to compute ν_T in the wake state of RANS method in the current study. This model is a semi-empirical model based on model transport equations for the turbulence kinetic energy (k) and its dissipation rate (ε). In the derivation of the k-ε model, the assumption is that the flow is fully turbulent, and the effects of molecular viscosity are negligible. The standard k-ε model should be therefore valid for fully turbulent flows such as blade stall state as well as turbulent state in this research.

Regarding mesh

An O-Grid structured mesh is used to reach a reliable momentum distribution inside the Navier-Stokes domain (Figure 2a). Satisfying independency and Y^+ under 10% (near walls) are considered as main targets in mesh creation. After numerous attempts, the following described mesh meets our expectations. The mesh of the disc is structured as follow: 36 radial divisions from hub to tip, 72 azimuthal divisions, and 2 axial divisions. To get more accurate flow around the disc, it is merged inside a cylinder. The cylinder (doesn't show in Figure 2) is modeled and meshed using an O-Grid structured mesh. A hybrid mesh is used for the wind tunnel. Quad-dominant method is used to make surface grids and tetra-mixed method is used for the meshing volume of the test section. The volume mesh is condensed around the cylinder from the compressor nozzle to the collector nozzle. Input and output channels are meshed in a structured way. They are added to the test section to complete model of the wind tunnel. Finally, the cylinder carrying the disc is

merged inside the wind tunnel to accomplish the final grid containing 6084344 cells and 1710361 nodes.

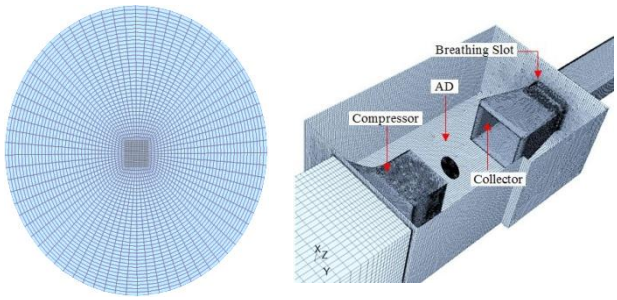

(a) **(b)**

Figure 2. Grid generated: (a) Structured mesh of the actuator disc (AD), (b) hybrid mesh of the DNW/LLF wind tunnel

UDF/AD Technique

In actuator disc simulations boundary layers are not explicitly simulated, but their effect is taken into account via the lift and drag coefficient. The actuator disc exerts a force on the flow, acting as a momentum sink. This force is explicitly added to momentum equations [27]:

$$\int_{\gamma}\frac{\partial}{\partial t}(\rho\vec{u})\mathrm{d}\gamma+\int_{\partial\gamma}\rho\vec{u}\vec{u}.n\mathrm{d}S=-\int_{\partial\gamma}p.n\mathrm{d}S+\int_{\partial\gamma}\mu\nabla\vec{u}.n\mathrm{d}S+\int_{\xi\cap\gamma}\vec{f}\mathrm{d}\xi \quad (5)$$

which are written in a weak form, because the force leads to a discontinuity in pressure (equation 5). The flow domain and the actuator disc domain are introduced by γ and ξ to integrate, respectively. The volume forces $\vec{f}$ is acting on $\xi\cap\gamma$. Momentums needed for the AD model in the current study are calculated from Equations (6), (7) and (8) along *x*, *y* and *z* directions, respectively. An analytical combination of these equations with airfoil formulations acts as momentum terms in Navier-Stocks equations, where $(f_x, f_y, f_z)=\vec{f}$. This mathematical calculation of momentums is the basic difference between this study and research of Rethore et al. [22].

$$f_x=-\rho V_{rel}{}^2 Bc\left(C_l\sin\varphi-C_d\cos\varphi\right)(4\pi rt)^{-1}\sin\theta \quad (6)$$

$$f_y=-\rho V_{rel}{}^2 Bc\left(C_l\sin\varphi-C_d\cos\varphi\right)(4\pi rt)^{-1}\cos\theta \quad (7)$$

$$f_z=-\rho V_{rel}{}^2 Bc\left(C_l\cos\varphi+C_d\sin\varphi\right)(4\pi rt)^{-1} \quad (8)$$

$$\varphi=\tan^{-1}\left(\frac{u}{V_{rel}}\right),\ V_{rel}=\sqrt{\left(r.\omega+\left(v.\cos\theta-w.\sin\theta\right)\right)^2+u^2} \quad (9)$$

In Equations (6 - 9), ρ is air density, V_{rel} is relative velocity of the local airfoil, *B* is blade number, *c* is the local chord, C_l and C_d are lift and drag coefficient of the airfoil, φ is flow angle, θ is azimuthal angle of the element at the disc plan, *r* is local radius of the element, *t* is rotor thickness, ω is angular velocity of the rotor (44.45 rad.s^{-1}), *u* , *v* and *w* are axial (*z*-direction), vertical (*x*-direction) and horizontal (*y*-direction) velocity of central node of the element, respectively, *x* and *y* are vertical and horizontal distance from the element center to the rotor center at the disc plan. In these equations, lift and drag coefficient are called from the local 2D airfoil analysis. Velocity components of each element (*u*, *v*, *w*) are measured from the Navier-Stocks domain in the iteration process by using UDF codes. Variables in Equations (6), (7) and (8) are calculated via Equations (9).

Designation of the blades is based on variable chord and pitch angle along spanwise that are interpolated for consideration in the calculation. 2D aerodynamic coefficients (C_l and C_d vs angle of attack (AOA)) inputs of the AD simulation are represented in literature [18, 22]. These coefficients are interpolated as a function of AOA. For transitional parts where there are no aerodynamic coefficients available, linear functions are used to interpolate C_l and C_d. To take into account complete geometry of the blade, AOA is calculated according to radial position; pitch angle and velocity components of the located element.

Calculating momentums and returning them on central nodes of elements are accomplished via User-Defined-Functions inside FLUENT solver. It is introduced as UDF/AD technique in this research. UDF/AD iterated inside the laminar formulation of Navier-Stokes equations (described in section 4) is introduced as AD-LNS model. Iteration of UDF/AD inside Reynolds averaged formulation of Navier-Stokes equations is introducing as AD-RANS model. Next section of this paper illustrates the results of both UDF/AD models compared to a direct model carried out on the MEXICO experiment by [15]. The direct model was organized and solved by TAU code under RANS turbulent model. The TAU code has been started more than a decade ago at DLR in Göttingen [28]. For more detail about the DLR-TAU code, the reader is referred to literature [29]. Full geometry of the rotor without wind tunnel geometry (a free air model) is iterated inside TAU environment reintroducing as TAU/DM technique in this paper. For more details on this model, the reader is referred to the origin of the described model [15].

Numerical results

Upstream side of the rotor is introducing as induction region where the wind flow is induced by the rotor. This causes to reduce the velocity nearby the rotor plan. Downstream side of the rotor is introducing as down-wake region where the induced wind flow leaving the

turbine is excited by the rotor. Three physical behaviors of the wake are studied in both induction and down-wake regions. Rotor wake is discussed for the three test states of the experiment: turbulent state (10 $m.s^{-1}$), rotor design state (15 $m.s^{-1}$) and blade stall state (24 $m.s^{-1}$). The rotor wake is studied for axial, centrifugal and spiral behaviors. Axial behavior describes the straight forward velocity of the wake flow, centrifugal behavior declares center escaping of the wake flow and spiral behavior describes the swirl velocity of the wake around the rotor axis. Axial, radial and azimuthal components of the flow velocity describe the axial, centrifugal and spiral behaviors of the wake, respectively. Distance from 1×D (D = 4.5 m, rotor diameter) in the upstream up to1.34×D in the downstream is assumed as near wake of the rotor where the PIV data are measured.

Axial traverses

Figures 3, 4 and 5 describe behavior of the wake in the axial direction at turbulent, design and blade stall states, respectively. Axial traverses at the design state (15 $m.s^{-1}$) are illustrated in Figure. 4. They show that axial behavior of the wake is well followed by both AD-LNS and AD-RANS models. At both turbulent and design state, the same results are also computed by Shen et al. [30] via actuator line technique on MEXICO rotor, particularly in the inner spanwise. The wake at the design state along axial traverse behaves more or less similar to that at the turbulent state. Since, it's completely different at the blade stall state (see Figure 5). This is because of unequal distribution of wind speed among turbulent, design and blade stall states. Results of all UDF/ADs and TAU/DM approaches follow the behavior of PIV data. However they are not trustable enough in the down-wake region.

Because the circulation varies along the blade span, vorticity is shed into the wake in a continuous fashion from the trailing edge. Thus, each blade sheds a helicoidal sheet of vorticity. Therefore, data measured in axial direction are fluctuating as crossing the helicoidal shape. This phenomenon is well appeared while measuring the spiral behavior at the blade stall state (Figure 5e and 5f). These fluctuations are highly condensed at both turbulent and design states because of high tip speed ratio. They are not conspicuous enough at these states, because the MAS function absorbs high frequency transient fluctuations for smoothing the measurement. These fluctuations are captured by the TAU/DM technique in the down-wake region (see Figure 5e and 5f). They are also computed by actuator line technique [31]; however, better results obtained by TAU/DM. As described before, in UDF/AD approach, rotor is assumed as an infinite blade number turbine. Hence, it sheds a tube sheet of vorticity from the disc edge, which caused to compute an average of the fluctuations by UDF/AD approaches.

As indicated in Figure. 5, ability of all numerical computations is decreased along axial traverses at the turbulent state. This is because of high transient behavior of the flow in lower tip speed ratio. Upcoming wind speed of 24 $m.s^{-1}$ leads to an average of 14.51 degree of AOA on the blade spanwise. This causes to recall lift and drag coefficients from the stall region. An average of 8.22 and 3.51 degree of AOA on the blade is captured at turbulent and design states, respectively. This causes to recall aerodynamic coefficients from the inviscid region where lift and drag have a smooth slope behind the stall region. These are the sources of the steady behavior at both turbulent and design states, and the transient behavior at the stall state.

Radial Traverses

Rotor jet in upstream and downstream is introducing as induction jet and wake jet, respectively. Induction and wake jets are measured in +0.3 m and -0.3 m distance from the rotor plan, respectively. Stream tube has also divided to two domains: outer and inner. Flow in the outer domain does not cross the rotor, but affected by the rotor jet. Flow in the inner domain is crossing the rotor where extremely excited. The boundary between outer and inner domains is introducing as shear layer, where the vorticity magnitude is intensively raising up.

In Figures 6, 7 and 8, while we are moving from left diagrams to the right (for example from Figure 6a to 6b), significant mutation is happening. This is because of rotor-crossing from the induction jet to the wake jet. Axial, centrifugal and spiral behaviors of the wake along radial traverses at the turbulent state are illustrated in Figure 6. As a rotor crossing from Figure 6a to 6b, performance of each model is varied specially in ambient flow very close to the rotor.

In Figure 6 radial traverses in the turbulent state are in agreement with PIV measurements. But, it seems the mesh to be coarse for simulating centrifugal behavior via UDF/AD techniques. TAU/DM model shows a weakness for calculating the spiral behavior of both induction and wake jets.

Radial traverses of both induction and wake jets in design state are illustrated in Figure 7. As an overlook, it seems the UDF/AD approaches present good agreement with experiment, especially in reproducing axial velocity. A significant velocity drop in PIV traverse is seen at a radial position of about 1.2 m in Figure 7b. This indicates the occurrence of 'tip vortex' type vortex shedding from the transition zone between the DU and Risø airfoils. Figure 7d exhibits a peak for centrifugal velocity measured at the shear layer. In the shear layer flow is sucking out from the rotor domain with a maximum speed of 6.75 $m.s^{-1}$. This results to an enforced vacuum as a source of pressure reduction of the wake jet at the design state. TAU/DM model exhibits unsteady behavior as do not obey measured spiral velocity in both induction and wake jets.

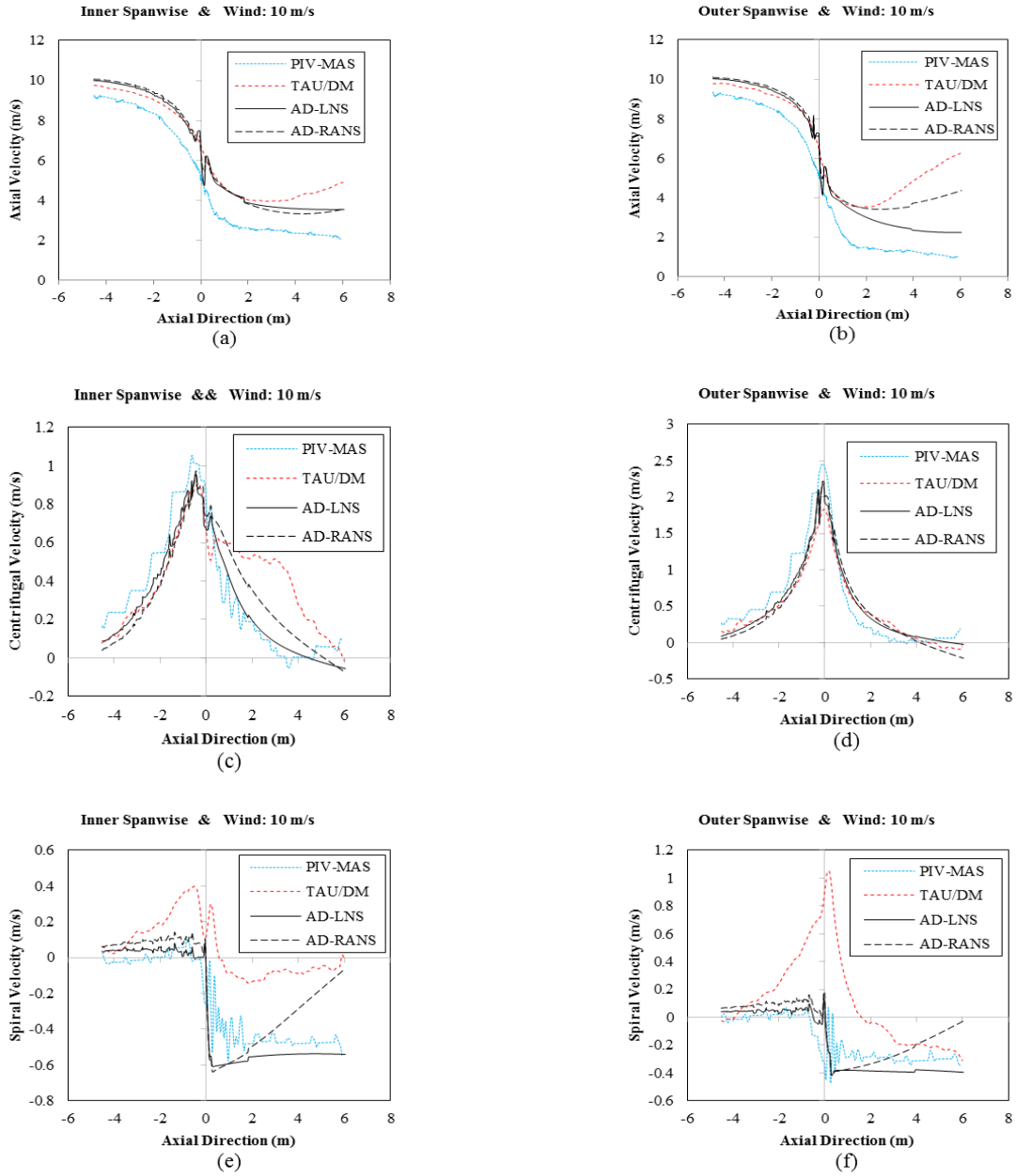

Figure 3. Axial traverses in wind speed of 10 m.s^{-1} for inner spanwise (r=1.377 m) and outer spanwise (r=1.848 m), (a) and (b) for Axial, (c) and (d) for centrifugal, (e) and (f) for spiral velocity

As a conclusion on Figure 7, both AD-LNS and AD-RANS approximately behaved the same in almost all diagrams, although AD-LNS shows better agreement than the others. AD-LNS estimates axial velocity of the wake jet, satisfactorily. It can also be concluded that the precision of all models increases as traverses are switching into the wake jet at the design state.

In Figure 8, wake traverses are not satisfactorily reproduced by computations. High transient flow at the blade stall state may need more developed mathematical approaches such as actuator line [30] and actuator surface [31] techniques to be captured. Diagrams show that ability of all techniques for estimating PIV data is rising up as flow crossing the rotor into the down wake jet. As a summary on Figure 8, for radial traverse it's found that discrepancy of numerical models at the stall state is more dramatic than that at both design and turbulent states. Axial and centrifugal behaviors of the induction jet are well captured by TAU/DM model. Axial and spiral behaviors of the wake jet are satisfactorily estimated by AD-LNS model.

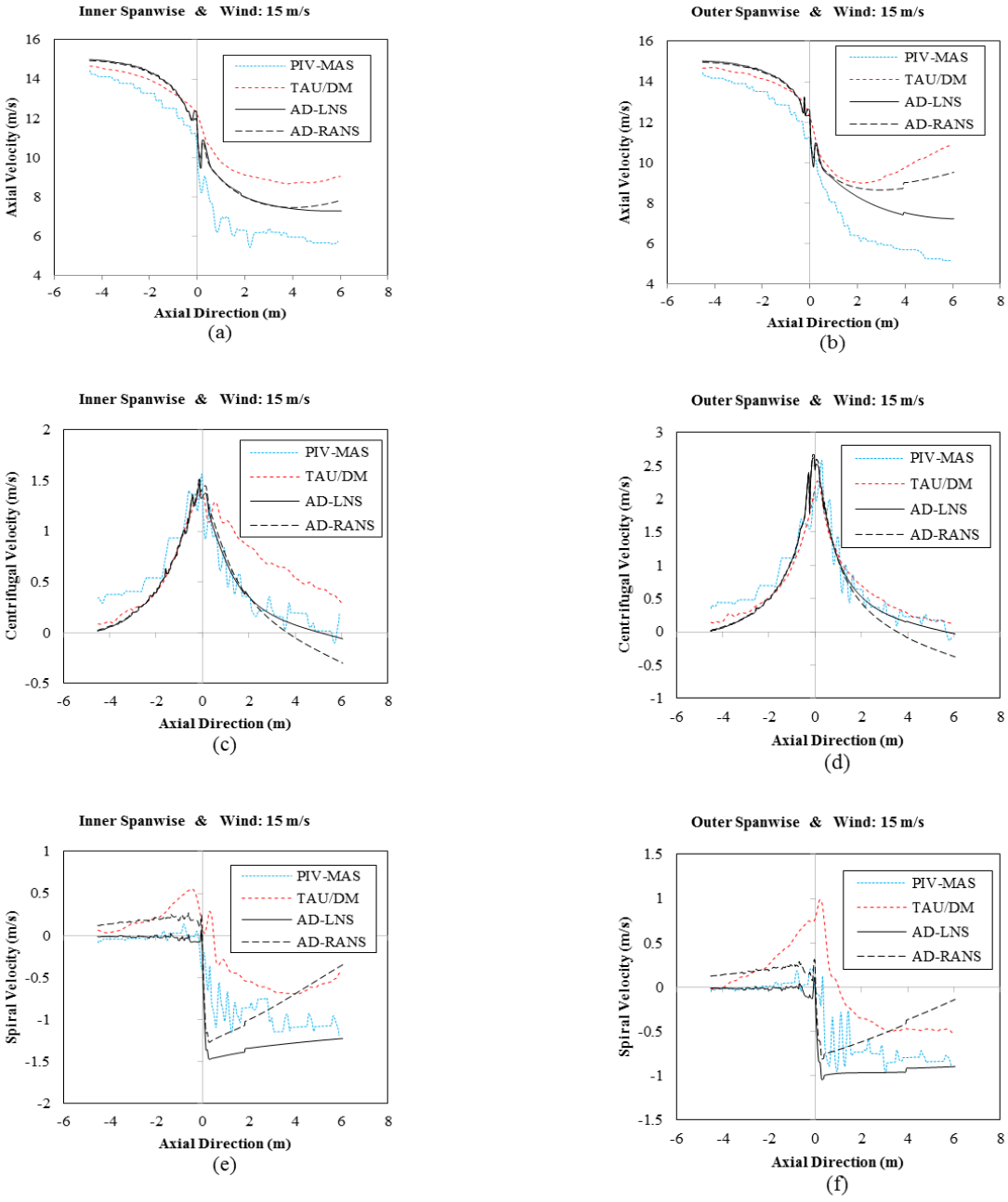

Figure 4. Axial traverses in wind speed of 15 m.s^{-1} for inner spanwise (r=1.377 m) and outer spanwise (r=1.848 m), (a) and (b) for Axial, (c) and (d) for centrifugal, (e) and (f) for spiral velocity

Wake Visualizations

As seen in Figure 2, test section of the wind tunnel is an open jet. The wind crosses the rotor origin in 7 m in front of the collector nozzle. An axial velocity plot in the horizontal plane is illustrated in Figure 9 for both AD-LNS (top contour) and AD-RANS (bottom contour) in the turbulent state. The wind jet shears the free air of the test section. The contours show that the wake in downstream is constricted in two regions. The first shrink occurs while the wake crosses the collector nozzle, where the flow is affected significantly by boundary layers. Second shrink occurs while the wake crosses the breathing slot. These effects seem to be the most considerable impact of the wind tunnel onto the wake.

The open jet test section is not symetric. The wall on the left has half of the distance to the rotor rather than the right wall. Therefore, bounday layers of the left wall is closer to the rotor than that of the right wall. The AD-RANS model is exageretly affected by boundary layers

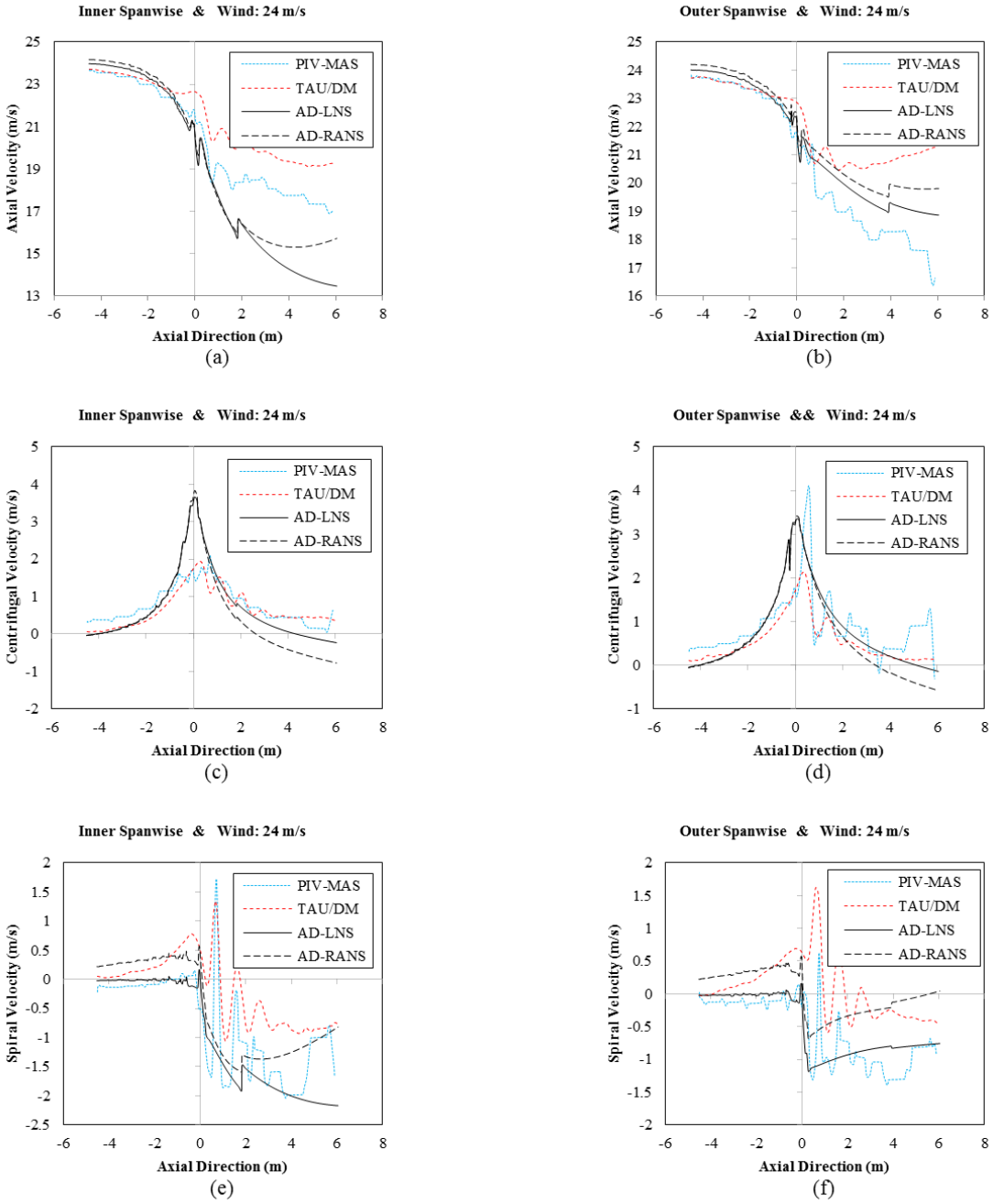

Figure 5. Axial traverses in wind speed of 24 m.s^{-1} for inner spanwise (r=1.377 m) and outer spanwise (r=1.848 m), (a) and (b) for Axial, (c) and (d) for centrifugal, (e) and (f) for spiral velocity

because of using the standard *k-ε* equations that is very sensitive to boundary layers [27]. This is leading to an inclination of the down wake to right side (bottom contour of Figure. 9). Actuator line technique in LES domain [30] and direct model in both steady state and DES domain [16] are in good agreement with AD-LNS technique in this study.

CONCLUSIONS

Combination of actuator disc and blade element analysis as a new technique to feed momentums inside a generalized actuator disc using UDF codes, UDF/AD, was presented. UDF/AD iterated in laminar Navier-Stokes domain and in Reynolds-averaged Navier-Stokes domain was introduced by AD-LNS and AD-RANS models, respectively. Both UDF/AD codes were computed on MEXICO rotor in the full geometry of the DNW/LLF wind tunnel and the wake results were

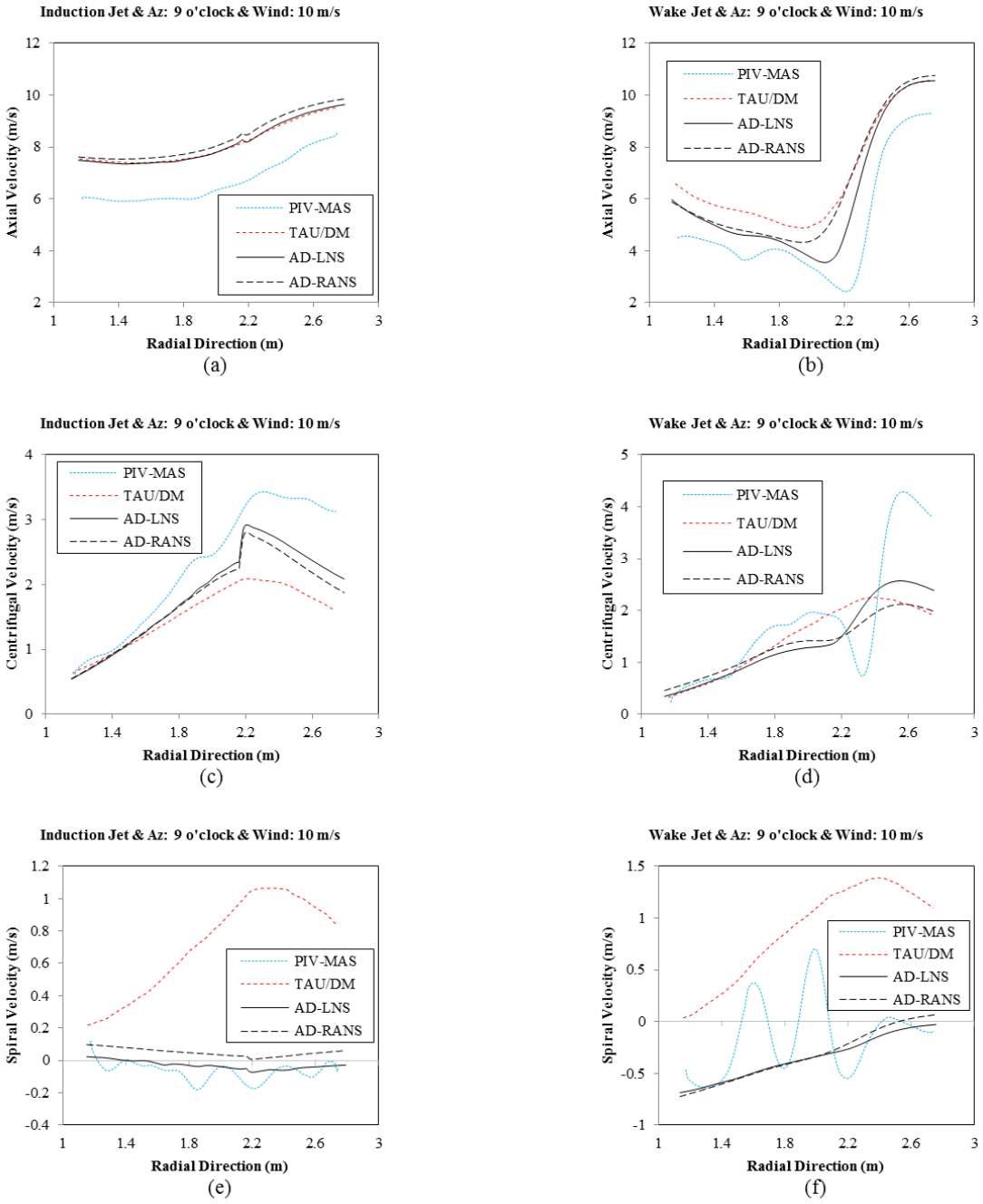

Figure 6. Radial traverses in wind speed of 10 m.s^{-1} for induction jet (the lefts) and wake jet (the rights), (a) and (b) for Axial, (c) and (d) for centrifugal, (e) and (f) for spiral velocity

compared with detailed results of a direct model called TAU/DM as well as other related research in the literature. They were validated via PIV measurements. The main results of this research are concluded as follows:

-Axial traverses were simulated better than radial traverses.Wake flow behavior in lower wind velocity (turbulent and design states) was more predictable than that in higher wind velocity (blade stall state).

-A constant upshift is computed for axial velocity almost in all computations, which is also observed in the other researches. More work should be focused on this problem, as it raises an issue with future open jet wind tunnel experiment of wind turbine wakes.

-Wakes released from inboard parts of the rotor were predicted more effective than that from the outboard parts.

-The AD-LNS approach showed more stability than the

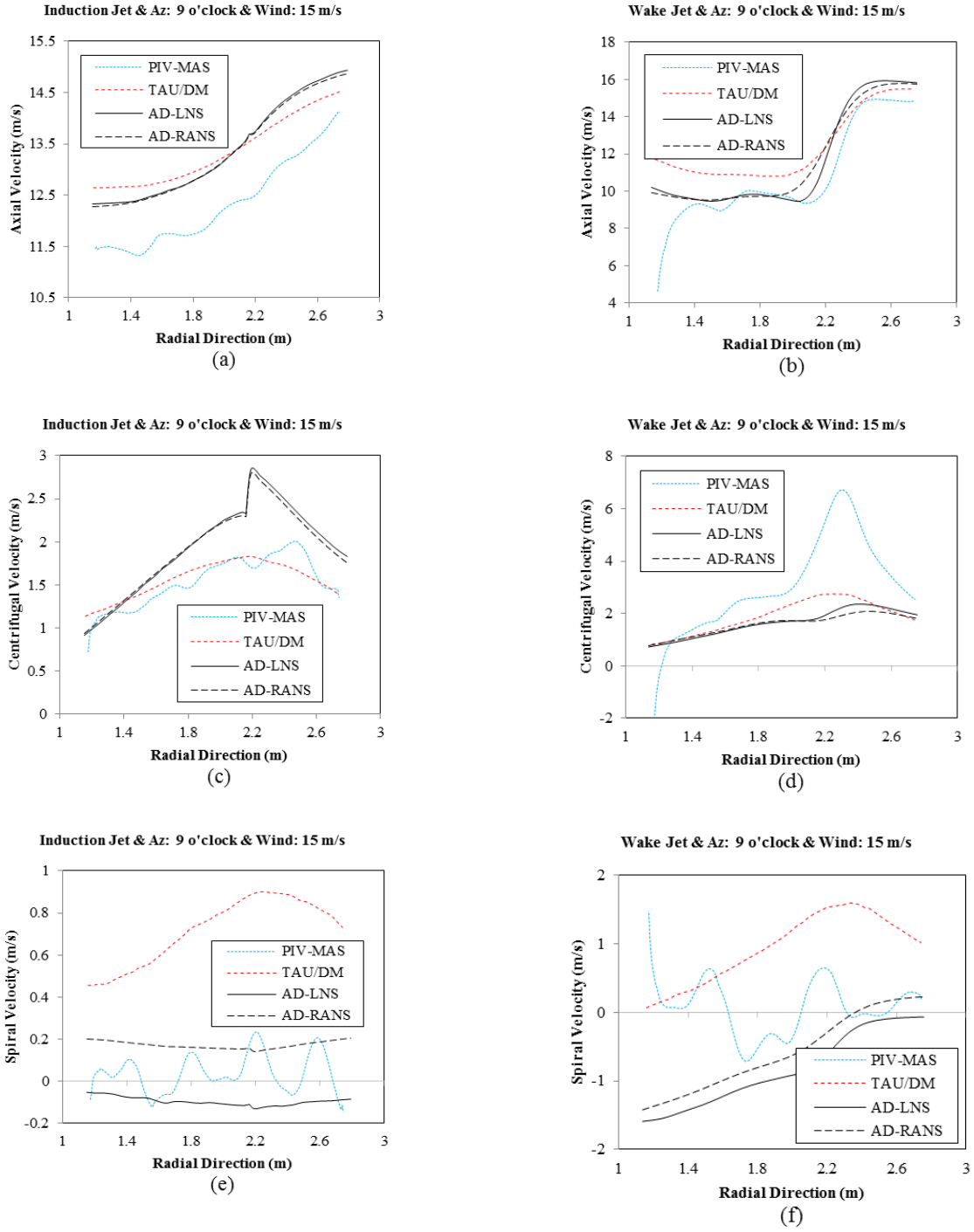

Figure 7. Radial traverses in wind speed of 15 m.s^{-1} for induction jet (the lefts) and wake jet (the rights), (a) and (b) for Axial, (c) and (d) for centrifugal, (e) and (f) for spiral velocity

other techniques while the PIV data cross the rotor from induction region to the down-wake region for axial traverses, as well as from induction jet to wake jet for radial traverses,

-Iteration UDF/AD model with laminar structure of the Navier-Stokes equations raised up as a reliable technique for rotor wake modeling in this study. The results showed that the effect of the wind tunnel on the near wake is not significant. But it is remarkable for the far wake.

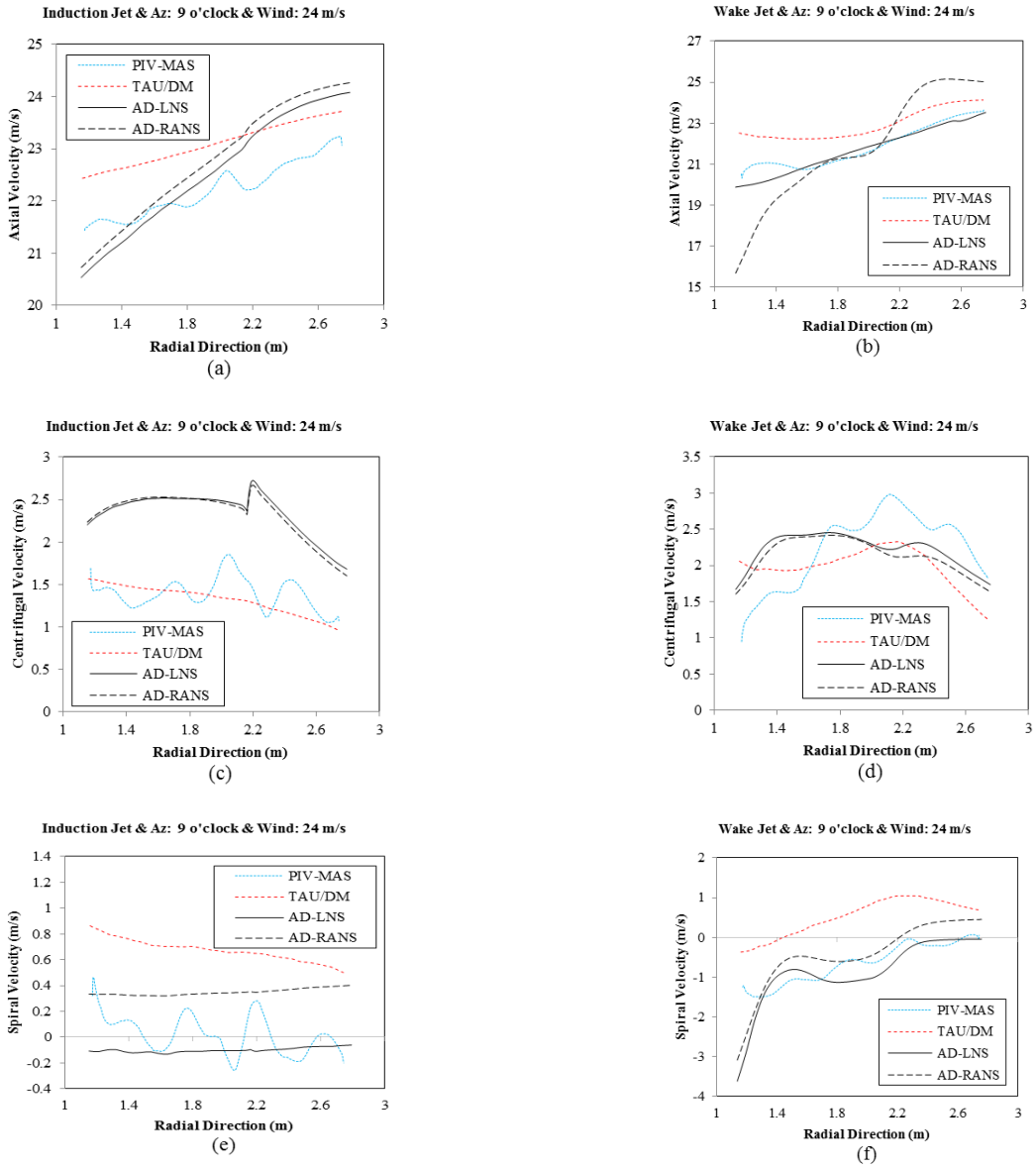

Figure 8. Radial traverses in wind speed of 24 m.s^{-1} for induction jet (the lefts) and wake jet (the rights), (a) and (b) for Axial, (c) and (d) for centrifugal, (e) and (f) for spiral velocity

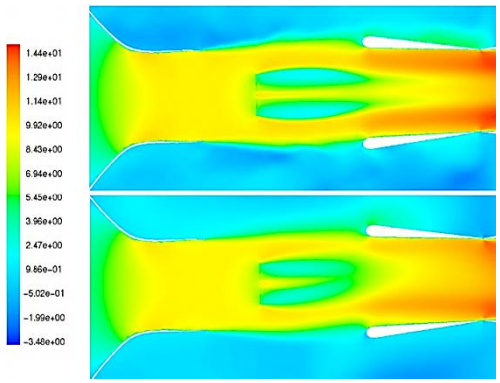

Figure 9. Instantaneaus axial velocity plot in the horizontal plan across the rotor origin for a wind speed of 10 m.s^{-1}

ACKNOWLEDGEMENT

We are very thanking full of University of Tehran, University of Shahrood and University of Applied Science, Kiel for funding the project and giving us scientific consultation.

REFERENCES

1. Hess, J.L. and A. Smith, 1967. Calculation of potential flow about arbitrary bodies. Progress in Aerospace Sciences, 8: 1-138.
2. Thomson, L.M.M., Theoretical Aerodynamics, 1973: Dover publications.

3. Conlisk, A., 1997. Modern helicopter aerodynamics. Annual Review of Fluid Mechanics, 29(1): 515-567.
4. Sørensen, N.N. and M.O. Hansen, 1998. Rotor performance predictions using a Navier-Stokes method. AIAA paper, 98: 0025.
5. Duque, E.P., M.D. Burklund and W. Johnson, 2003. Navier-Stokes and comprehensive analysis performance predictions of the NREL phase VI experiment. Journal of Solar Energy Engineering, 125(4): 457-467.
6. Duque, E. P. N., C. P. Van Dam and S. C. Hughes. 1999. Navier-Stokes simulations of the NREL combined experiment phase II rotor. 18th 1999 ASME Wind Energy Symposium, AIAA, pp. 99-0037.
7. Fletcher, T.M. and R.E. Brown, 2010. Simulation of wind turbine wake interaction using the vorticity transport model. Wind Energy, 13(7): 587-602.
8. Johansen, J., N. Sorensen, J. Michelsen and S. Schreck. Detached-eddy simulation of flow around the NREL phase-VI blade. in ASME 2002 Wind Energy Symposium. 2002. American Society of Mechanical Engineers.
9. Johansen, J. and N.N. Sørensen, 2004. Aerofoil characteristics from 3D CFD rotor computations. Wind Energy, 7(4): 283-294.
10. Prado, R.A., M.A. Storti and S.R. Idelsohn, 2002. Numerical Simulation of the 3D Laminar Viscous Flow on a Horizontal-axis Wind Turbine Blade. International Journal of Computational Fluid Dynamics, 16(4): 283-295.
11. Sørensen, N.N., J. Michelsen and S. Schreck, 2002. Navier–Stokes predictions of the NREL phase VI rotor in the NASA Ames 80 ft× 120 ft wind tunnel. Wind Energy, 5(2-3): 151-169.
12. Zahle, F. and N.N. Sørensen, 2011. Characterization of the unsteady flow in the nacelle region of a modern wind turbine. Wind Energy, 14(2): 271-283.
13. Vermeer, L., J.N. Sørensen and A. Crespo, 2003. Wind turbine wake aerodynamics. Progress in Aerospace Sciences, 39(6): 467-510.
14. Bechmann, A., N.N. Sørensen and F. Zahle, 2011. CFD Simulations of the MEXICO Rotor. Wind Energy, 14(5): 677-689.
15. Jeromin, A.a., A. P. , Full 3D computations of a rotating blade using unstructured grids, in IEA wind, MexNext meeting Forth 2010: Heraklion, Crete, Greece.
16. Rethore, P.E., Sørensen N. N. , Zahle F., Bechmann A., Madsen H., MEXICO Wind Tunnel and Wind Turbine modelled in CFD, in EWEA Brussels2011: Belgium.
17. Sumner, J., C.S. Watters and C. Masson, 2010. CFD in wind energy: the virtual, multiscale wind tunnel. Energies, 3(5): 989-1013.
18. Mahmoodi, E., A. Jafari, A.P. Schaffarczyk, A. Keyhani and J. Mahmoudi, 2014. A new correlation on the MEXICO experiment using a 3D enhanced blade element momentum technique. International Journal of Sustainable Energy, 33(2): 448-460.
19. Mikkelsen, R., Actuator disc methods applied to wind turbines, 2003, Technical University of Denmark.
20. Shen, W., R. Mikkelsen, J. Sørensen and C. Bak. Evaluation of the Prandtl tip correction for wind turbine computations (poster). in 2002 Global Wind Power Conference and Exhibition.
21. Ammara, I., C. Leclerc and C. Masson, 2002. A viscous three-dimensional differential/actuator-disk method for the aerodynamic analysis of wind farms. Journal of Solar Energy Engineering, 124(4): 345-356.
22. Rethore, P.E., Sørensen N. N. , Madsen H. A., Modelling the MEXICO Wind Tunnel with CFD, in IEA wind, MexNext meeting Forth,2010: Heraklion, Crete, Greece.
23. Boorsma, K., Schepers J. G., Description of experimental setup MEXICO measurement, ECN, Editor 2011: Netherlands.
24. Schepers, J. and H. Snel, 2007. Model experiments in controlled conditions. ECN Report.
25. G., S. Introduction on 2th meeting on IEA Task 29 MexNext. in 2th MexNext Meeting, IEA Task 29. 2009. Montreal, Canada.
26. Sematech, N., e-Handbook of Statistical Methods, 2012.
27. Sanderse, B., v.d.S. Pijl and B. Koren, 2011. Review of computational fluid dynamics for wind turbine wake aerodynamics. Wind Energy, 14(7): 799-819.
28. Gerhold, T., O. Friedrich, J. Evans and M. Galle, 1997. Calculation of complex three-dimensional configurations employing the DLR-TAU-code. AIAA paper, 167: 1997.
29. Schwamborn D., G.T., Heinrich R. , The DLR TAU Code: Recent Application in Research and Industry, in European Conference on Computational Fluid Dynamics, E.O. P. Wesseling, and J. Périaux, Editor 2006: eds. TU Delft, The Netherlands.
30. Shen, W.Z., W.J. Zhu and J.N. Sørensen, 2012. Actuator line/Navier–Stokes computations for the MEXICO rotor: comparison with detailed measurements. Wind Energy, 15(5): 811-825.
31. Shen, W.Z., J.N. Sørensen and J. Zhang. Actuator surface model for wind turbine flow computations. in 2007 European Wind Energy Conference and Exhibition. 2007.

Persian Abstract

DOI: 10.5829/idosi.ijee.2015.06.03.07

چکیده

در این مطالعه، مدل های عددی مختلفی محاسبه شده و با سرعت سنجی تصویری ذرات برای همبستگی خطی یک روتورتوربین بادی به قطر۴٫۵متر مقایسه شد.پروژه توربین بادیMEXICO در سه حالت آزمایش متداول با سرعت های بادی ۱۰، ۱۵و۲۴ متر بر ثانیه انجام شده است. برای بررسی خطوط نزدیک روتور، روش Navier-Stokes (LNS) آرام و مدل توربولنت Reynolds averaged Navier-Stokes به همراه تکنیک actuator disc (AD) محاسبه شده است و سپس با مدل مستقیم گرفته شده از مقاله TAU/DM به عنوان تکنیک روتور کامل مقایسه شده است. مومنتم دیسک محرک با استفاده از توابع تعریف شده ی کاربر(UDF) در جریان تعریف شده به عنوان تکنیک UDF/AD در این مقاله محاسبه شده است. نتایج با جزییات کامل با اندازه گیری های PIV بحث شده و مقایسه شده است.